Near-threshold electronic excitation by electron impact of multilayer physisorbed N_2 and CO

R. M. Marsolais, M. Michaud, and L. Sanche
Groupe du Conseil de Recherches Médicales du Canada en Sciences des Radiations, Faculté de Médecine, Université de Sherbrooke, Sherbrooke, Québec, Canada J1H 5N4
(Received 11 July 1986)

Electronic excitation of N_2 and CO condensed (i.e., physisorbed) on a metallic substrate has been investigated by high-resolution electron-energy-loss (HREEL) and low-energy electron-transmission (LEET) spectroscopies in the incident energy range 0—19 eV. The HREEL results yield a more complete picture of the spin-forbidden vibronic bands of the solids than previously available from photon spectroscopies. All levels are found to be shifted down by a few tens of meV and broadened with respect to the gas-phase values. As expected, Rydberg states are absent from such spectra. The LEET experiments provide a measurement of inelastic transitions near the electronic excitation threshold. By recording the second energy derivative of LEET spectra, transitions having a strong cross section near threshold are identified by the sharp structure they produce. These are the $a\ ^3\Pi$ state in CO and, in N_2, the $A\ ^3\Sigma_u^+$ and $B\ ^3\Pi_g$ states and a new previously unobserved vibronic band near 12 eV. The magnitudes of thresholds cross sections in the solid phase are discussed in terms of single-electron—molecule scattering mechanisms.

I. INTRODUCTION

Electron scattering by isolated atoms and molecules has been a subject of intensive research for more than half a century.[1] Reasonably successful theories have yielded a fairly complete understanding of the mechanisms responsible for the magnitude and energy dependence of the measured cross sections. At high energy (>1000 eV), the electron-molecule interaction or electronic cross section can be described within the first Born approximation.[2] This leads to the concept of generalized oscillator strength, which is similar to the optical oscillator strength in the limit of small momentum transfer. In this limit, it is nonzero only when the optical selection rules for the electric dipole transitions allow it. As the incident electron energy is decreased, the contribution of optically forbidden transitions (i.e., electric quadrupole, octupole, etc.) to the cross section relative to the dipole transitions is enhanced and the exchange interaction favors transitions involving a change of multiplicity. Furthermore, the target orbitals are strongly perturbed by the presence of a nearby electron and the first Born approximation ceases to be valid. At very low energies (<100 eV), and especially near the excitation threshold, the multiple scattering within the molecule, the perturbation, and the exchange interactions are no longer negligible. These perturbations not only account for the excitation of optically forbidden states but have been observed to lead to energetically highly localized phenomena such as compound state formation, Wigner cusps, and virtual state effects.[3]

Central to the understanding of electron scattering in condensed systems is the knowledge of the modifications of the known electron—single-target interactions generated by the presence of neighboring targets or a given surface. Although important information can be obtained for thermal or nearly thermal energies from mobility experiments,[4] it is only recently that it has been possible to address such fundamental questions over a wider energy range (0—30 eV). Low-energy electron-transmission (LEET) spectroscopy,[5,6] variable-energy high-resolution electron-energy-loss (HREEL) spectroscopy,[7,8] and electron-stimulated desorption[9] (ESD) have all served to generate information on electron scattering by condensed molecules whose interactions with electrons are well understood in the gas phase.

Molecular nitrogen and carbon monoxide have been molecules of choice for such investigations since a wealth of information exists in the literature on their scattering properties and because in the condensed phase they formed molecular solids having vibrational and electronic properties perturbed only weakly by dispersive forces. So far, the energy dependence of the vibrational and libration cross sections have been studied over the 1—30-eV range.[8,10,11] These experiments were particularly successful in demonstrating the occurrence of shape resonances in condensed N_2 and CO. Differences between the two phases in the compound states were attributed to modifications in the long-range polarization force and in the partial-wave content of the resonant electron.

The present work is devoted to an investigation of electronic excitation in N_2 and CO condensed on platinum and niobium in an energy region where the incident and inelastically scattered electron wave is most likely to be perturbed by neighbor molecules and/or the presence of a metal surface (i.e., near the threshold for electronic excitation). Scattering near threshold strongly depends on the angular momentum of the outgoing electron and the strength of the long-range potentials. Electron resonance existing near threshold can also be affected by a change in the width function and the possible appearance of a long-range dipole potential in the excited state capable of binding an electron. These effects are expected to be modified in the solid phase where the inelastic electron wavelength at threshold should be coupled to the surrounding since it

 ©1987 The American Physical Society

is much longer than the lattice parameter. Coherent (elastic) scattering of the electron prior to and after the energy-loss event may also play a crucial role.

In this paper we present high-resolution energy-loss spectra for electrons of 16 and 13.5 eV incident on condensed N_2 multilayer films and of 19 eV incident on CO films. A modification of the LEET spectroscopy allows the observation of the electronic excitations near threshold in the incident energy range 0—14 eV for various film thicknesses. The paper is organized as follows. A brief description of the experiments is given in Sec. II. Experimental results are presented and discussed in Sec. III, which we have divided in sections. Section III A is concerned with HREEL results on electronic excitations and their interpretation. In Sec. III B we present the general features observed in the LEET spectra over the entire energy range (0—14 eV) and interpret the structure qualitatively. Section III C is devoted to the results of an investigation of the inelastic energy region where electronic excitation plays a crucial role. In Sec. III D basic concepts of LEET spectroscopy are introduced in order to analyze more quantitatively the data of Sec. III C. Section III E contains a brief discussion of the mechanism known to be responsible for the threshold features appearing in the gas phase. We then discuss the applicability of the theories to the condensed state.

II. EXPERIMENT

The HREEL spectrometer has been described in details elsewhere.[8] It basically consists of a hemispherical monochromator, which produces the monoenergetic electron beam incident on a cooled (20 K) solid sample, and a hemispherical energy analyzer, which collects electrons reflected in a well-defined solid angle. The monochromator can be rotated from 14° to 70° from the normal to the sample and the analyzer is fixed at 45°. Typical currents arriving on the target range from 0.5 to 5 nA for a corresponding overall resolution extending from 10 to 30 meV full width at half maximum (FWHM). The spectrometer is located in a bakeable ion-cryopumped ultrahigh-vacuum system capable of sustaining working pressures within the 10^{-11}-Torr range.[12]

The LEET spectrometer is of the type described in previous articles.[13] It basically consists of a trochoidal electron monochromator[5,14] which generates a magnetically collimated electron beam of a few nA at about 60 meV FWHM. The electron beam impinges at normal incidence on a metallic substrate held at 18—20 K. The latter is connected to a fast (time constant of 50 μs) sensitive electrometer which serves to measure the transmitted current. Special care was exercised in the wiring in order to minimize current fluctuations caused by the cryogenic system, thereby enhancing the signal-to-noise ratio. The spectrometer is housed in ion- and titanium-pumped ultrahigh vacuum system reaching a base pressure of 10^{-10} Torr.

Doubly differentiated (DD-) LEET spectra are obtained as follows. A weak sinusoidal energy modulation of the incident electrons generates a modulation of the transmitted current whose first and second harmonics are proportional to the first and second energy derivative of the transmitted current, respectively. A lock-in amplifier, locked on the modulation frequency, detects in phase either one of these harmonics, and produces a signal equal to the rms value of their amplitude. The contribution of higher harmonics and derivatives, which causes spurious signals, is greatly reduced by keeping the modulation amplitude to a minimum (30—80 mV) and by using appropriate high-pass filters at the input.

In both instruments, the calibration of the energy is based on the transmission spectra. When the energy is swept upward, the transmitted current is null until it rises rapidly near the zero of incident energy. This sharp rise is termed "injection," and its sharpness increases with the resolution until it is limited by potential fluctuations on the surface of the film. In the LEET spectrometer we take the steepest slope of the sharp rise as the zero of energy with respect to the vacuum level.

Except for HREEL experiments on N_2, for which we used niobium, the substrate was a 2.0×1.0 cm^2 polycrystalline platinum ribbon, 0.20 mm thick, supplied by the Ventron Corporation with a stated purity of 99.98%. In both devices it was press fitted to the cold end of a closed-cycle refrigerated cryostat from which it is electrically isolated by a ceramic plate and sapphire balls. The temperature is maintained constant and monitored by a thermocouple (Au at 0.07% Fe versus Chromel) secured to the copper block supporting the substrate. The substrate is cleaned by resistive heating (at about 1500 K) each time the film is renewed. It is now established that, after repetitive resistive heating, the Pt microcrystals preferentially reorient with the [111] direction normal to the plane of the surface and a strong azimuthal disorder.[15]

The films are formed by vacuum depositing controllable amounts of the gas under investigation, which is admitted in the chamber through a tube ending in front of the substrate. The latter is connected at the other end to a valve which isolates it from the gas-handling system. This enables us to control the exposure, hence the thickness of the film. Two complementary methods have been used in the present work to estimate the coverage, which is usually expressed in monolayers (ML), although the uniformity of the deposition is difficult to ascertain. We first identified the LEET spectrum of a single layer, either during the slow evaporation of a multilayer film caused by a slow temperature sweep through the sublimation point or by continuously exposing the substrate to the sample gas just above its bulk sublimation temperature corresponding to a partial pressure in the 10^{-10}-Torr range.[13,16] Next we measured the minimum amount of gas required to reproduce that spectrum and then assumed that the subsequent monolayers add up with no change in sticking coefficient. The second method is based on quantum size effects (QSE).[16,17] These give rise to series of peaks and dips in LEET spectra characteristic of the number of layers. A set of peaks (and dips) fades away and is replaced by a new one each time a monolayer is added to the film. We shall see that such interference patterns appear in the transmission spectra of condensed N_2 and CO. A calibration of the thickness is thus obtained by monitoring the variation of QSE features with thickness. With this method the estimated accuracy is better

than 15% for thicknesses ranging from 0 to 15 ML. We used Matheson Research grade gases with stated purity of 99.99% for CO and 99.9995% for N_2. We varied the thickness from 0 to 15 ML.

Because of charge accumulations in the films and a slow desorption (and degradation in the case of CO), the long integration times required by second-energy-derivative techniques limited DD-LEET recordings to thicknesses smaller than 10 ML. In all experiments, the temperature was maintained constant near 18 K, which is a few degrees below the sublimation temperature (21 K for N_2 and 20.5 K for CO, at 10^{-10} Torr) in order to optimize the order in our films.[13,18]

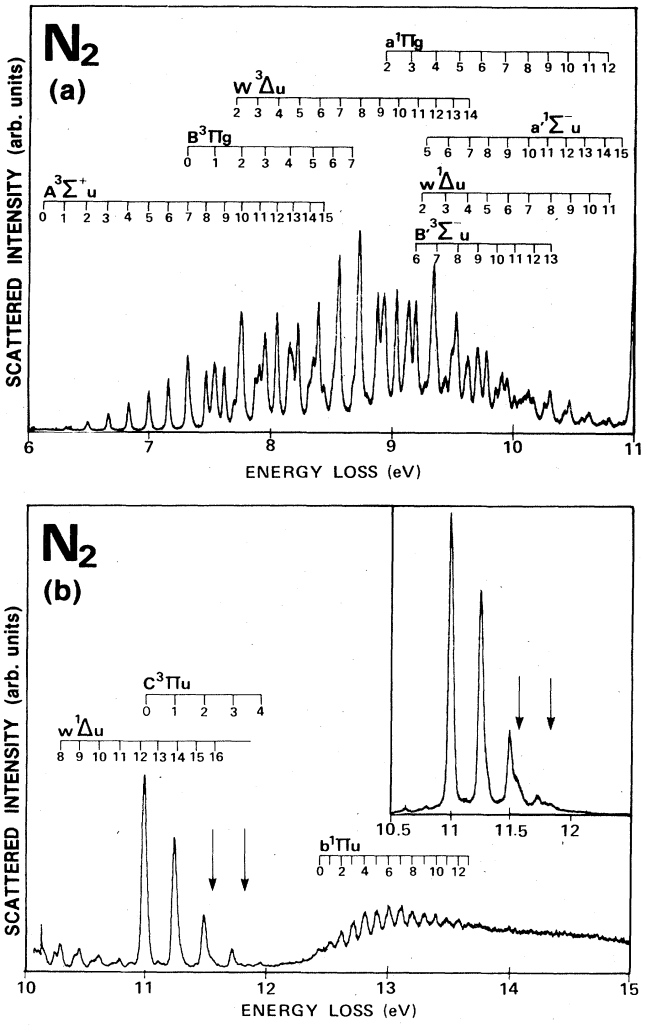

FIG. 1. (a) HREEL spectrum of N_2 on Nb in the range 6—11 eV. The incident energy is 16 eV. (b) HREEL spectrum of N_2 on Nb in the range 10—15 eV. The incident energy is 16 eV. The arrows indicate the position of two weak peaks whose enhanced visibility at 13.5-eV incident energy (inset) is attributed to a resonance.

III. RESULTS AND DISCUSSIONS

A. Energy-loss spectra

Energy-loss spectra for 15 layers of N_2 on Nb and CO on Pt are shown in Figs. 1 and 2, respectively. The incident energy is 16 eV for N_2 and 19 eV for CO; in both cases, the incident angle is 45°. At these energies the magnitude of each of the probed states is small compared to that of the total scattering cross section. According to multiple scattering theory,[11] this condition ensures negligible perturbation from multiple scattering losses in the observed spectra. The intensity of energy-loss peaks is found to increase steadily with thickness up to about 3 ML to become subsequently almost thickness independent. These energy-loss peaks are about three orders of magnitude smaller than the elastic one. We list in Tables I and II the energy of the losses together with their spectral assignment for N_2 and CO, respectively. Published values in the gas and solid phases are also listed for comparison.

Below about 10.5 eV the present energy-loss spectra are qualitatively similar to those recorded in the gas phase at the same primary energy and at about 90° from the primary beam.[19] In N_2 we even observe the presence of two weak peaks near 11.6 and 11.82 eV (Fig. 1) similar to those found in the gas phase by Vichon *et al.*[20] who attributed them to the existence of a previously undetected valence state. The excitation functions of these states exhibited oscillatory structure centered at about 2 eV above each respective threshold indicating the presence of a resonance mechanism and explaining the increased visibility in the 13.5-eV incident-energy spectrum inserted in Fig. 1. Above 11.5 eV, in a region where an abundance of Rydberg states appears in the gas phase,[21] we only observe the $b\ ^1\Pi_u$ valence state in N_2, and a few weak peaks in CO.

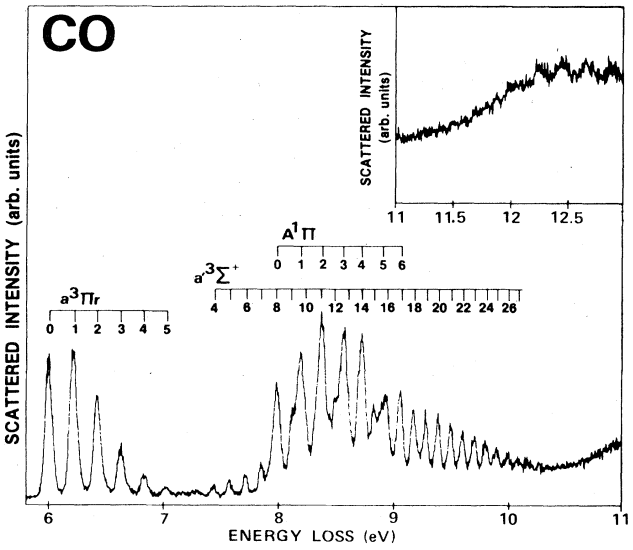

FIG. 2. HREEL spectrum of CO on Pt in the range 5.9—13 eV. The incident energy is 19 eV.

TABLE I. Measured energy (eV) for the energy-loss peaks of Figs. 1(a) and 1(b) for N_2. A spectral assignment to the lines is given in the second column with $A = A\,^3\Sigma_u^+$, $B = B\,^3\Pi_g$, $W = W^3\Delta_u$, $a = a\,^1\Pi_g$, $B' = B'\,^3\Sigma_u^-$, $w = w\,^1\Delta_u$, $C = C\,^3\Pi_u$, and $b = b\,^1\Pi_u$. Comparison is made between these values and the spectroscopic data available in the literature for both gaseous and solid N_2.

Present HREEL	Spectral assignment	Gaseous N_2 optical a,b	c	Gaseous N_2 others d,e	f,g,h	i,j	Solid N_2 optical k,l	m
6.332	*A*1	6.347		6.34				
6.510	*A*2	6.521		6.52				
6.678	*A*3	6.691		6.69				
6.848	*A*3	6.858		6.86				
7.010	*A*5	7.022		7.02				
7.170	*A*6	7.182		7.18				
7.330	*A*7	7.339						
7.35	*B*0	7.354		7.35	7.353			
7.480	*A*8	7.492						
7.548	*B*1	7.565		7.56	7.565			
7.630	*A*9	7.641						
7.702	*W*2		7.728					
7.765	*B*2	7.773		7.77	7.772			
	*A*10							
7.885	*W*3		7.906					
7.915	*A*11	7.929						
7.960	*B*3	7.977		7.97	7.977			
8.058	*W*4		8.080					
8.16	*B*4	8.178		8.17	8.177			
8.19	*A*13	8.201						
8.232	*W*5		8.250					
8.32	*A*14	8.333						
8.355	*B*5	8.375		8.37	8.374			
8.400	*W*6		8.418					
8.450	*A*15	8.460						
8.520	*B*6	8.568		8.56	8.568			
8.560	*W*7		8.585					
8.68	*B*7	8.758		8.75				
8.728	*W*8		8.750					
8.800								
8.880	*W*9		8.910				8.846	*w*0
8.930	*a*2				8.96	8.903		
9.032	*W*10		9.068				9.033	*w*1
9.128	*a*3				9.155	9.106		
9.188	*W*11				9.215			
	*B'*6		9.233					
9.23	*w*2		9.273			9.214	9.221	
9.265	*a'*5		9.287					
9.332	*a*4				9.35	9.305		
	*W*12				9.37			
9.365	*B'*7		9.401					
9.442	*w*3		9.457			9.398	9.405	
	*a'*6		9.459					
9.48	*W*13				9.51			
9.522	*a*5				9.54	9.502		
9.53	*B'*8		9.565					
9.62	*w*4		9.693			9.580	9.585	
	*W*14				9.65			
	*a'*7		9.628					
(9.70)	*B'*9		9.727					
9.705	*a*6				9.71			
9.775	*w*5		9.818			9.760	9.770	
	*a'*8		9.795					
9.848	*B'*10		9.886					
9.898	*a*7				9.92			

TABLE I. (*Continued*).

Present HREEL	Spectral assignment	Gaseous N_2 optical a,b	Gaseous N_2 optical c	Gaseous N_2 others d,e	Gaseous N_2 others f,g,h	i,j	Solid N_2 optical k,l	Solid N_2 optical m
(9.94)	$a'9$		9.959					
9.948	$w6$		9.994				9.946	
10.008	$B'11$							
10.09	$a8$				10.10			
10.11	$a'10$		10.119					
10.125	$w7$						10.120	
10.165	$B'12$							
10.26	$a9$				10.28			
	$a'11$	10.277						
10.305	$w8$						10.290	
	$B'13$							
10.425	$a10$							
	$a'12$		10.432					
10.462	$w9$						10.457	
10.575	$a'13$		10.585					
(10.60)	all				10.626			
10.625	$w10$				10.654		10.62	
10.74	$a'14$		10.735					
10.76	$a12$				10.799			
10.7888	$w11$				10.815			
10.88	$a'15$		10.883					
11.002	$C0$		11.029	11.03	11.041			
11.11	$w13$				11.133			
11.250	$C1$		11.275	11.28	11.289			
11.42	$w15$				11.457			
11.492	$C2$		11.520	11.52	11.521			
11.575	$w16$							
11.723	$C3$				11.754			
12.448	$b0$	12.500		12.500		12.46	12.500	12.474
12.525	$b1$	12.579		12.575		12.55	12.579	12.568
12.620	$b2$	12.665		12.663		12.66	12.668	12.661
12.720	$b3$	12.754		12.750		12.74	12.761	12.762
12.815	$b4$	12.839				12.85	12.856	12.855
12.910	$b5$	12.981				12.96	12.953	12.968
13.010	$b6$	13.061		13.062		13.05	13.052	13.064
13.108	$b7$	13.156		13.156		13.15	13.150	13.157
13.205	$b8$	13.258		13.260		13.25	13.248	13.257
13.300	$b9$	13.346		13.345		13.35	13.343	13.352
13.398	$b10$	13.437		13.435		13.45	13.436	13.446
13.490	$b11$	13.529				13.55	13.528	13.364
13.580	$b12$	13.617				13.64		13.651
13.670	$b13$	13.704				13.71		13.713

[a]Reference 44. For all states but the *b* progression.
[b]Reference 45. For the *b* progression only.
[c]Reference 46.
[d]Reference 33. Trapped electron method (for the *A*, *B*, and *C* states).
[e]Reference 47. High-energy electron spectroscopy (for *b* progression only).
[f]Reference 20. EEL spectroscopy (*w* and *a* states).
[g]Reference 37. Metastable states experiments (for the *B* states only).
[h]Reference 48. For *a* and *B'* progressions only, EEL spectroscopy.
[i]Reference 23. Zero phonon line of *a* and *w* states.
[j]Reference 49. For the *b* progression only.
[k]Reference 27.
[l]Reference 24. For the *w* states only. The observed Davydov splitting of the *w*1, *w*2, and *w*4 levels is not indicated and we only give the average value.
[m]Reference 26. For the *b* states only.

TABLE II. Measured energies (eV) for the energy-loss peaks of Fig. 2. A spectral assignment is given to the peaks in the second column with $a = a\,^3\Pi$, $a' = a'\,^3\Sigma^+$, and $A = A\,^1\Pi$. Comparison is made with the spectroscopic data available in the literature for both gaseous and solid CO.

Present HREEL	Spectral assignment	EEL gas[a]	Optic gas[b]	Optic solids[c]
6.00	$a0$	6.010	6.010	
6.215	$a1$	6.223	6.222	
6.420	$a2$	6.432	6.430	
6.630	$a3$	6.637	6.635	
6.830	$a4$	6.839	6.837	
7.02	$a5$	7.035	7.034	
7.43	$a'4$	7.447	7.453	
7.57	$a'5$	7.586	7.592	
7.710	$a'6$	7.723	7.729	
7.845	$a'7$	7.858	7.863	
7.980	$A0$	8.028	8.028	7.914-7.972
8.10	$a'9$	8.120	8.125	
8.195	$A1$	8.211	8.211	8.102-8.173
8.37	$A2$	8.391	8.391	8.297-8.357
8.47	$a'12$	8.495	8.501	
8.56	$A3$	8.566	8.566	8.496-8.544
8.715	$A4$	8.727	8.737	8.694
8.82	$a'15$	(8.850)	8.855	
8.88	$A5$	8.903	8.903	8.864
8.92	$a'16$	8.963	8.968	
9.045	$a'17$	(9.075)	9.079	
	$A6$	9.065	9.065	9.028
9.160	$a'18$	(9.184)	9.188	
9.27	$a'19$	9.290	9.294	
9.38	$a'20$		9.398	
9.49	$a'21$		9.499	
9.59	$a'22$	(9.596)	9.598	9.511-$d16$
9.69	$a'23$	9.694	9.695	
9.79	$a'24$	(9.788)	9.790	9.740-$d18$
9.88	$a'25$	9.881	9.882	9.835-$d19$
9.98	$a'26$	(9.971)		9.92-$d20$
10.06	$a'27$	(10.058)		10.011-$d21$

[a]Reference 50. Parentheses indicate that these lines are not observed but extrapolated.
[b]Reference 44.
[c]Reference 24. The Davydov splitting of the A levels is indicated. The observed d states are mentioned as a possible assignment for the last levels.

Our measurements also show that the position of all the peaks are shifted down by a few tens of meV with respect to the gas-phase values. The shift is more important (>25 meV) for high values of the vibrational quantum number. The energy resolution of the electron beam in our spectra (about 20 meV) allows us to detect a broadening of the energy levels whose actual width can be easily estimated if we assume that the observed width results from the convolution of two Gaussian line shapes. We then find for well-resolved vibronic peaks in N_2, 26, 40, 30, 37, 35, 47, and 51 meV for the $A\,^3\Sigma_u^+$, $B\,^3\Pi_g$, $W\,^3\Delta_u$, $^1\Pi_g$, $w\,^1\Delta_u$, $C\,^3\Pi_u$, and $b\,^1\Pi_u$ states, respectively; and for CO, 30, 14, and 31 meV for the $a\,^3\Pi$, $a\,'^3\Sigma^+$, and $A\,^1\Pi$ states, respectively. Peak broadening is expected to be due to multiple scattering,[8,11] faster decay of the excitation, and dispersion. The absence of significant dependence of the position of the peaks on the angle of incidence, along with the small broadening of the vibronic structure, indicates little dispersion for the excitons.

In terms of the band structure of these compounds, we are probing excitonic states lying within the band-gap region. Indeed, photoemission measurements on solid N_2 showed the presence of three valence bands ($3\sigma_g$, $1\pi_u$, and $2\sigma_u$) as expected, and a conduction band some 15 eV above the $3\sigma_g$ valence band.[22] Optical measurements had already revealed progressions of narrow excitonic bands in the band gap, such as the series $w\,^1\Delta_u$ and $a\,^1\Pi_g$ identified by Boursey *et al.*[23] They measured their band width to be 17 and 45 meV, respectively, together with a rigid shift of all the levels of 50 meV with respect to the gas phase, as measured with the zero phonon line of each level. Data on the solid phase of carbon monoxide is scarce although a wealth of information is available on CO physisorbed or chemisorbed on various metal substrates, most of which points to a severe distortion of the CO orbitals caused by the presence of the metal. uv absorption mea-

surements[24] in solid CO revealed the $A\,^2\Pi$ (7.9—10 eV) and $d\,^3\Delta$ (9.6—10.2 eV) bands. A splitting of the $A\,^1\Pi \leftarrow X\,^1\Sigma^+$ transitions is observed and attributed to Davydov splitting.[25] The gap should thus be at least 10.5 eV wide in CO. As for nitrogen, the optical data give a larger shift of the excitonic levels than that observed in the present experiment. The discrepancy may come from the fact that photons mainly probe direct interband transitions ($k=0$) whereas electrons will induce transverse transitions, leading to vibronic broadening corresponding to a convolution over the dispersion curve and the density of states.

Perturbative changes are thus observed in the low-lying electronic excitation levels of N_2 and CO upon condensation. Yet Rydberg states are absent from our spectra, as we would expect since they possess effective radii comparable to lattice dimensions. According to Buxton and Duley,[26] remnants of these states in the solid would influence the observed transitions, leading, for instance, to an irregular spacing of the peaks. Our data, however, as well as the optical data of Boursey and Roncin,[27] show that the peaks are regularly spaced, which indicates minimal perturbation from Rydberg states.

B. General features of transmission spectra

LEET and DD-LEET spectra for N_2 and CO in the 0—14-eV energy range are presented in Figs. 3 and 4, respectively. In both figures the bottom curve corresponds to the LEET spectrum while the top curve(s) corresponds to the DD-LEET spectra. The DD-LEET spectra turn out to be highly structured over the entire energy range and the two molecules show striking similarities not so apparent in the LEET spectra.

The first set of peaks in N_2 between 0 and 2.4 eV is characterized by fairly evenly spaced (280 meV) peaks which are present even at submonolayer coverage. HREEL measurements on thin[10,28] and thick[8,10,29] films of N_2 on a metallic substrate have shown that the vibrational cross section is large in the 0—2-eV energy range. The results were attributed to the presence of a $^2\Pi_g$ shape resonance.[3,30] Furthermore, more refined measurements[8,10,29] for levels $v=1,2,3$ indicate that this resonance produces oscillatory structure or peaks in the excitation function of these states which is thought to originate from vibrational motion of the temporary N_2^- ion. These peaks are spaced by the same energy as in the present transmission experiment. All these facts thus suggest that the structure observed between 0.8 and 2.4 eV in N_2 is caused by the same N_2^- state. The same structure in CO may also originate from the $^2\Pi$ state[31] of CO^- or may simply reflect excitations of the vibrational states of the electronic ground state.

Whereas the 0—2.4-eV peaks are not appreciably displaced in energy with thickness, the second set of peaks (from 2.4 to about 5 eV), especially in nitrogen, is composed of oscillations whose amplitude and number depend critically on the thickness. Such variations are indicative of QSE, namely, interferences of the electron wave function inside the film caused by reflections at the film boundaries.[16,17] QSE peaks are, however, close, and most probably mixed, to the resonance structure at lower energy. This entire quasielastic energy region is now being examined in the frame of a single theoretical model.[32] In the present work, we focus our analysis on the higher-energy region, where electronic transitions near the excitation threshold dominate.

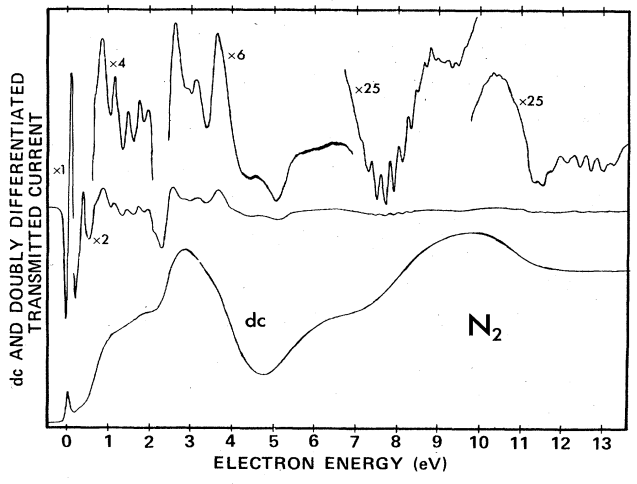

FIG. 3. LEET spectrum (bottom curve) on N_2 on Pt together with its DD-LEET spectrum (top curve). Various sections of the DD-LEET spectrum have been amplified by a factor indicated near every section. The modulation amplitude was 60 mV.

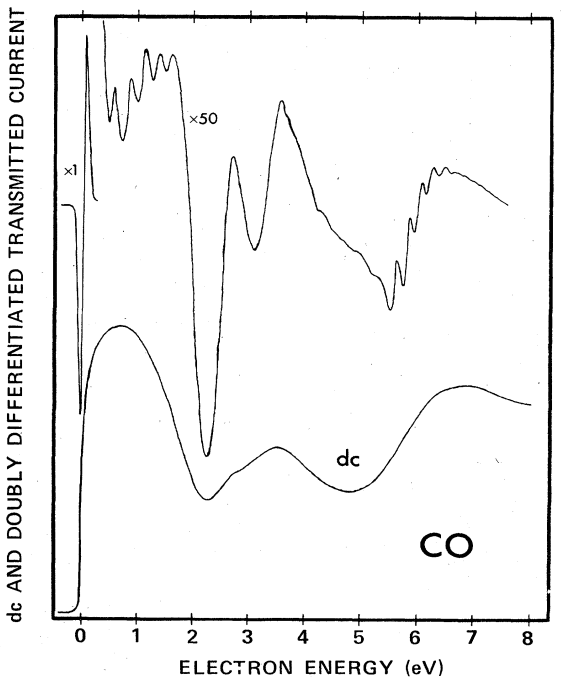

FIG. 4. LEET spectrum (bottom curve) of CO on Pt together with its DD-LEET spectrum (top curve). The modulation amplitude was 75 mV.

C. Near-threshold excitation spectra

The thickness dependence of DD-LEET spectra is shown in Figs. 5 and 6 for N_2 and in Fig. 7 for CO. The spectra in N_2 cover the entire energy range from 6 to 14 eV, while the investigation in CO was limited to energies below about 7.5 eV because we noticed an important deterioration of the film during the long integration times required to record second-energy-derivatives spectra above 7 eV. We indicate in the figures the position of the energy-loss peaks of Figs. 1 and 2, with the zero of energy calibrated with respect to the vacuum level as defined in Sec. II. We find a difference between the low-coverage limit (<3 ML) and higher-coverage limit, corresponding to a gradual transition from the absorbed-molecule regime to the bulk solid. In the latter, molecules feel perturbations typical of the condensed phase although the metallic substrate may still influence the transmission spectra through its image potential and the electron reflectivity at its surface. We shall confine our discussion to the higher-coverage limit, although most of the concepts are directly transferable to the lower coverages.

The N_2 DD-LEET spectra in Fig. 5 reveal the presence of at least two series of peaks, one barely visible series below 7.2 eV and one series of strong and narrow peaks above 7.2 eV. The position of the steepest slope on the low-energy side of each peak matches quite closely the $A\,^3\Sigma_u{}^+$ and the $B\,^3\Pi_g$ progressions. The relative amplitudes are also quite consistent with the HREEL amplitudes, even though the incident energy is different. A striking similarity is observed between our results and trapped-electron spectra in the gas phase.[33] The peaks above 8.5 eV also match the $a\,^1\Pi_g$ but there is apparently no trace of the Δ states. The spectra in Fig. 6 also consist of at least two series. The $C\,^3\Pi_u$ progression can be made to coincide with the minima in the observed structure but above 11.8 eV the progression of peaks cannot be attributed to any known electronic state. Their width (140 meV) is somewhat larger than that of the other peaks. They probably originate from an optically forbidden state having a strong cross section near threshold but normally hidden by Rydberg states in gas-phase HREEL spectra.

The DD-LEET spectra for CO in Fig. 7 show a single series of peaks spaced by about 200 meV. It is easily attributed to the $X\,^1\Sigma^+ \rightarrow a\,^3\Pi$ transitions provided that the zero of electron energy inside the film is taken to be a few hundred meV below vacuum. We shall once again take the position of each peak to be given by the middle of the sharp rise on the low-energy side of each peak, although the position of the peaks is harder to assess as the thickness increases: peaks tend to become mere shoulders, leaving only a sharp rise on the low-energy side. Notice that this sharp rise covers about 0.10 eV, which is a little more than the sharp rises in N_2 and definitely more than the instrumental resolution. The position of the peaks clearly depends on the thickness of the film. As the thickness is gradually increased, there is no significant change up to about 1 ML, then all peaks suddenly shift down in energy to reach a minimum near 2 ML (0.09 eV below). Subsequently they shift slowly upward, in a manner similar to an image-potential law, to reach

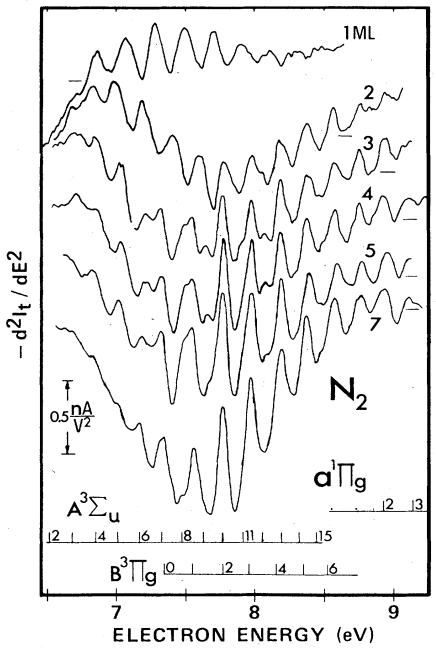

FIG. 5. DD-LEET spectra of N_2 on Pt as a function of thickness. The modulation amplitude was 40 mV. The energy losses ($X\,^1\Sigma_g{}^+ \rightarrow A\,^3\Sigma_u{}^+$, $X\,^1\Sigma_g{}^+ \rightarrow B\,^3\Pi_g$, and $X\,^1\Sigma_g{}^+ \rightarrow a\,^1\Pi_g$) obtained in the HREEL spectrum of Fig. 1 are also indicated with the zero of energy adjusted to the zero of transmission experiments as defined in the text.

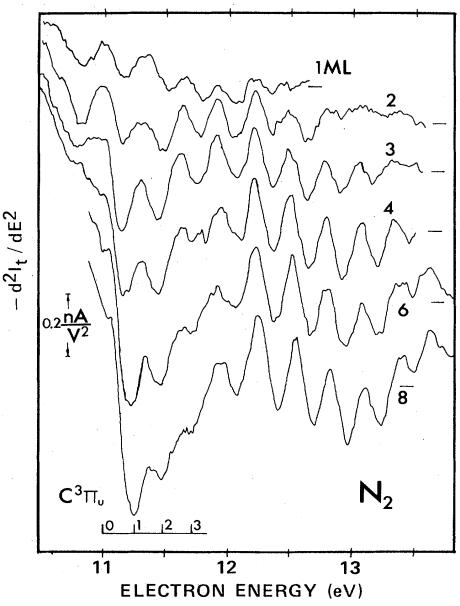

FIG. 6. DD-LEET spectra of N_2 on Pt as a function of thickness in the energy range 10.5—13.5 eV. The modulation amplitude was 40 mV. The energy losses corresponding to the $X\,^1\Sigma_g{}^+ \rightarrow C\,^3\Pi_u$ transitions as found in the HREEL spectrum of Fig. 1 are indicated.

asymptotic values above 10 ML (about 0.09 eV above the submonolayer values). These asymptotic values yield a rigid shift of the levels of about −0.30 eV with respect to the vacuum level.

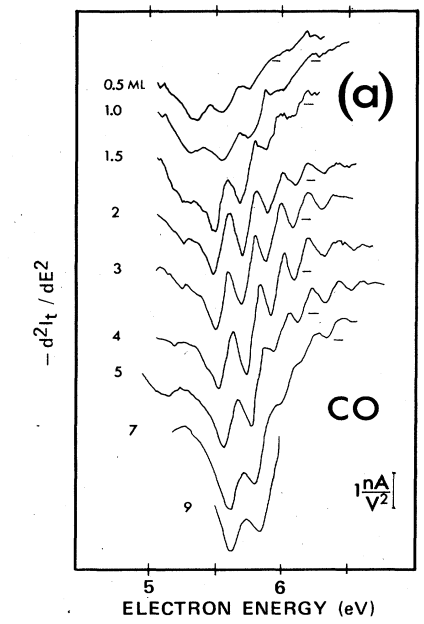

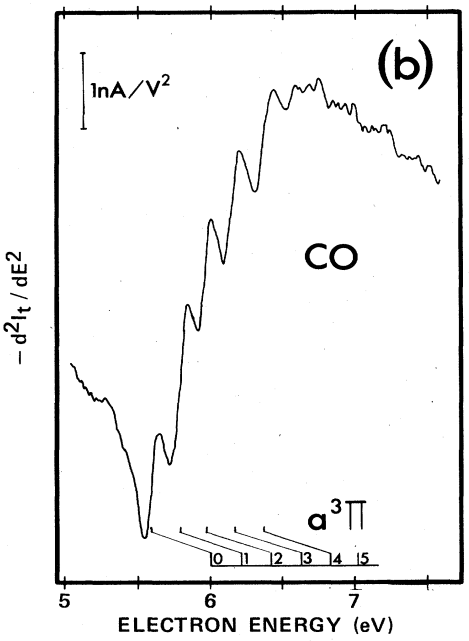

FIG. 7. (a) DD-LEET spectra of CO on Pt for various thicknesses. The modulation amplitude was 40 mV. (b) CO spectrum for a thickness of 5 ML. The $X\,^1\Sigma^+ \rightarrow a\,^3\Pi$ excitonic levels observed in the HREEL experiments are indicated.

D. Interpretation of LEET spectra above 5 eV

A recent interpretation of the LEET spectra has been given in terms of the band structure of the condensate.[34] In such a picture, the ensemble-averaged quasielastic and inelastic differential cross section for a given channel within the solid takes the form

$$\frac{d\sigma}{d\Omega}(E_i,E_f \leftarrow E_i) \propto |\langle \mathbf{k}_f,E_f,A_f \,|\, T \,|\, \mathbf{k}_i,E_i,A_i \rangle|^2 D(E_f)[1-f(E_f)] , \quad (1)$$

where T is the transition matrix, $\mathbf{k}$ and E are the wave number and the energy of the electron, respectively, A symbolically represents a set of quantum numbers to characterize the state of the solid before (i) or after (f) the scattering event, $D(E_f)$ is the occupancy function of these states. We can represent the current density at position $\mathbf{r}$ inside the film and final energy E' from initial electron energy E by the variable

$$\mathbf{J}\left[E',\mathbf{r};E,\sum d\sigma/d\Omega,R,R'\right] ,$$

where R and R' represent the reflection coefficients at the vacuum and metal surfaces, respectively, and where $\sum d\sigma/d\Omega$ means that $\mathbf{J}$ depends explicitly on all possible elastic and inelastic scattering events in the range of energy E to E'. For a two-level process involving a single inelastic channel, at the incident energy E, the electron faces a quasielastic channel (which takes into account small phonon losses) and an inelastic one. For the case of interest, the latter involves the creation of an exciton of energy E^* and the transmitted current can be expressed as an integral over J_z, the z component of $\mathbf{J}$ perpendicular to the metal surface,[35]

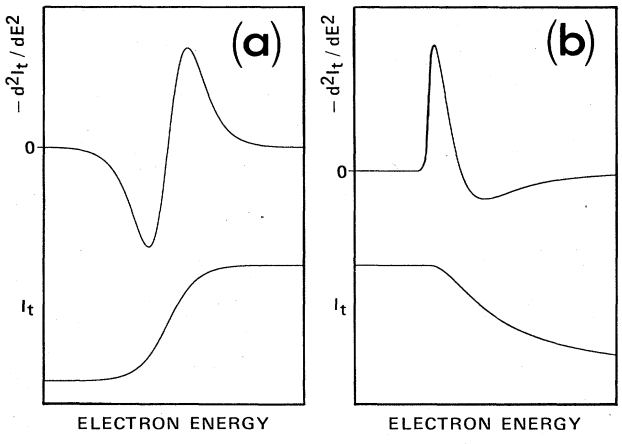

FIG. 8. (a) A hypothetical rapid increase in transmitted current (bottom) caused by well-defined threshold and the corresponding second energy-derivative signature (top). (b) A hypothetical drop in transmitted current caused by a drop in reflection coefficient at the film vacuum boundary (bottom) and its corresponding second energy-derivative signature (top).

$$I_t(E)=\int_{-\infty}^{E} dE' \int ds\{\langle[1-R'(E)]J_z(E,0;E,d\sigma(E)/d\Omega,d\sigma(E,E'\leftarrow E)/d\Omega,R(E),R'(E))\rangle + \langle[1-R'(E')]J_z(E',0;E,d\sigma(E,E'\leftarrow E)/d\Omega,d\sigma(E')/d\Omega,R(E'),R'(E'),R(E),R'(E))\rangle\}\ , \quad (2)$$

where $\mathbf{r}=0$ represents the metal surface. The surface integration formally extends to the entire surface, although it is effectively limited to an area of the order of the beam size. $d\sigma(E)/d\Omega$ and $d\sigma(E')/d\Omega$ are quasielastic cross sections, while $d\sigma(E,E'\leftarrow E)/d\Omega$ is the inelastic cross section.

Rapid changes in the energy dependence of J_z, through $d\sigma/d\Omega$, R, or R', are expected to result in sharp fluctuations in $I_t(E)$ via integral (2). Thus, whenever the electron energy changes by a large value over a narrow energy range the reflection coefficient R also changes by a large amount, causing sharp structure to occur in $I_t(E)$ through J_z. This situation occurs at the threshold of the creation of an exciton of energy E^* since at the threshold energy E the electron energy changes abruptly from E to $E-E^*$ causing R to increase from $R(E)$ to $R(E-E^*)$ by an increase in refraction (Snell's law). This rise can be followed by a decrease when $E=E^*$ because the inelastically scattered electron can now escape to vacuum. At the electronic excitation threshold, J_z in integral (2) therefore change rapidly over a narrow energy range due to variations in $d\sigma/d\Omega$ given by Eq. (1). According to this equation, sharp variations in $d\sigma/d\Omega$ are most likely to occur if the transition matrix T is strong at threshold. In this case, when $D(E)$ suddenly increases above the band edge, T forces considerable magnitude into $d\sigma/d\Omega$. Both situations considered here can lead to sharp structure in I_t although, depending on the position of the band edge (V_0), the shape and energy of the structure in DD-LEET spectra can be different, as demonstrated by a mathematical simulation using Eq. (2). According to the preceding argumentation, for a negative V_0 either or both mechanisms will produce, as depicted in Fig. 8(a), a step in transmitted current which will appear whenever $E=V_0+E^*$. The DD-LEET spectral features will be characterized by an S-shaped fluctuation with a steep rise in the middle. This situation corresponds to the case of CO whose second-energy-derivative features are referenced to a value below vacuum with $V_0=-0.3$ eV, a value consistent with the earlier estimate of -0.5 eV.[36] Moreover, the shape of the feature supports this possibility.

The case of nitrogen calls for another type of explanation with a positive V_0 in accordance with the previously determined value of $+0.8$ eV.[36] The fact that the excitonic features are referenced to the vacuum level suggests a fluctuation originating in the reflection coefficient at film-vacuum interface. Indeed, the reflection coefficient is unity when $E'<0$ and decreases with energy when $E'>0$. Thus, as the incident energy increases, a small drop in transmitted current appears whenever $E=E^*$ (since $E'=E-E^*$) because the inelastically scattered electron can now escape the film. This behavior produces structure in the DD-LEET spectra of N_2 resembling the curve on top of Fig. 8(b). The sharpness of the structure observed is an indication that the reflectivity must decrease rapidly above the vacuum level. Hence, despite the facts that V_0 is well above the vacuum level ($V_0=+0.8$ eV),[36] and that Eq. (1) disfavors inelastic events bringing the electron in the energy gap, our data shows that such events are non-negligible. It is therefore plausible that the decrease in intensity of J_z at $E=E^*$ may be due to electronic transitions coupled to vacuum states. Clearly, the mechanisms discussed occur with different intensities in the film and the strength of the features generated depends on several factors such as the intensity of the transition matrix involved, the density of final states, or simply the sign of V_0.

Calculations based on both dc and DD spectra using Eq. (2) were made[35] in order to give a numerical assessment of the cross sections. We found that the inelastic cross section ought to increase very rapidly in the first few hundred meV above each threshold in order to give rise to the observed spectra. Yet this rise at threshold cannot be too strong because it would entail a larger fluctuation of transmitted current, observable in the direct spectrum. Moreover, saturation of current by energy losses to the first vibronic level at the detriment of the following ones is not observed experimentally. The energy dependence of the total cross section for metastable state formation in gas-phase CO and N_2 has been measured by Newman, Zubek, and King.[37] It exhibits a gradual but rapid increase above threshold which saturates smoothly. By feeding the magnitude of the measured cross sections in Eq. (2), we can reproduce our spectra when we use a slower rise. In fact, both the dc and the DD spectra reveal that the overall increase in transmission is directly related to changes in the total cross section. These latter include at least the first five excitonic levels and indicate that the cross section keeps on increasing well beyond threshold. The energy-loss threshold occurs near or slightly below the steepest slope on the low-energy side of each maximum. It is also found that too slow a rise yields shoulders instead of peaks for the levels on the steep background slope in the DD spectrum. Other energy dependencies of the cross sections could in principle be invoked to fit our data, some of which requires a delicate balance between elastic and inelastic amplitudes.

E. Mechanisms of strong threshold cross sections

Electron-impact experiments in gaseous N_2 and CO show a sharp threshold for many electronically excited levels. The results of Swanson *et al.*[38] on carbon monoxide indicate that the $X\,^1\Sigma^+\rightarrow a\,^3\Pi$ transitions have very large cross sections at threshold. The metastable excitation measurements of Newmann, Zubek, and King[37] on CO and N_2 also show steep rises of the excitation function for the $a\,^3\Pi$ states of CO and the $B\,^3\Pi_g$ states of N_2. These are precisely the states which we can easily identify in our spectra. It is also known that polar molecules, such

as HCl, possess extremely sharp and narrow peaks in many of their excitation functions near threshold.[39]

Current theoretical models to explain the origin of such threshold effects bear on two mechanisms. One model is based on a distortion[40] or a resonant scattering of the S wave, which would then not be supported by the centrifugal barrier of the molecular potential as in a shape resonance. The enhancement of the incident electron wave function in the neighborhood of the molecule would originate from the existence of a virtual bound state, whose capability to bind an electron depends on the internuclear distance. Hence resonances can appear when vibrations are included. In the other model[41] the long-range dipole potential plays a crucial role in the enhancement of the wave function. The latter is greatly modified in the presence of a critical dipole potential, namely, a dipole just about to bind an electron. This model can predict a sharp peak at threshold which has a counterpart in the elastic channel. Resonances near threshold are conductive to effects on both the elastic and the inelastic cross sections, such as Wigner cusps or simply an enhanced elastic cross section in the vicinity of the inelastic threshold. Long-range potentials are also thought to have important bearing on the electron scattering cross section at threshold even in molecules such as CO (small permanent dipole moment) and N_2 (no permanent dipole moment).

The condensed state of molecules is expected to perturb the threshold effects essentially via a distortion of the long-range potential. An electron impinging on the condensate feels an image potential resulting from the polarization of all the molecules in the film. The symmetry of this potential is different from that between an electron and a single molecule. Once in the film, the electron experiences rather localized potentials at lattice sites with a fairly uniform potential between them, as recently shown in experiments and LEED calculations in the 0—12-eV range for the elastic reflection of electrons from Ar films.[42] The individual molecular long-range potential is therefore screened by the dielectric response of the solid. The localization of the electron wave function required by the previously mentioned mechanisms is thus hindered. One can also argue that any localization will be shorter lived in the solid due to coupling to neighboring molecules. We therefore expect to observe in the present experiment a strong suppression of threshold effects. Surprisingly, a simple inspection of the LEET spectra of both N_2 and CO in the inelastic region suggests large values for the inelastic cross sections in the first eV or so above threshold. This is even more so when we take into account the fact that the inelastically scattered electron can return back to vacuum if its final energy is above the vacuum level and that the transmitted current does not increase linearly with the inelastic cross section because the competition between scattering events produces a leveling-off effect.[13,35] Thus, these results and the sharp and narrow structure observed in the DD spectra combined with simple calculations provide evidence for the occurrence of large cross sections near threshold whose rise is spread out over hundreds of meV. This *does not mean,* however, that sharp peaks in the cross section occur near threshold since these would appear in the LEET spectra or at least give rise to DD-LEET features much larger and with more oscillations than what is actually observed.

Even though fine structure near threshold appears absent in the condensed state, mechanisms responsible for the large values of the cross section persist. Because of the screening of the long-range portion of the electron-molecule potential in condensed N_2 and CO, mechanisms other that those depending on the dipole interaction must be invoked to explain the present result. The existence of electron resonances near the electronic excitation energy could therefore be responsible for the strong enhancement of the threshold cross section for excitation of the $A\,^3\Sigma_u^+$ and $B\,^3\Pi_g$ states N_2 caused by the decay of two core-excited shape resonances[43] labeled a' and a, respectively, in the gas phase. These anion states lie 1.5—2.0 eV above the threshold energy of these states and are therefore not contributing to the amplitude of the cross section slightly above threshold. In the condensed state, however, transient anions are displaced to lower energies by 0.8—2.3 eV due to electronic polarization and changes in symmetry.[29] It is therefore possible for the anion states band a' and a to fall within the threshold region in our experiment. A similar mechanism can be invoked to explain our results in condensed CO since it is isoelectronic with N_2. These arguments illustrate that electron scattering cross sections in gases may be altered by condensation, not only due to changes in the lifetime of transient anions but also due to the displacement of these resonances with respect to their decay channels.

[1]For a review of electron-molecule scattering, see *Electron-Molecule Interactions and their Applications,* edited by L. G. Christophorou (Academic, New York, 1984), Vol. 1; and *Electron-Molecule Collisions,* edited by Isao Shimamura and Kazuo Takayanagi (Plenum, New York, 1984).

[2]M. Inokuti, Y. Itikawa, and J. E. Turner, Rev. Mod. Phys. **50**, 23 (1978); and M. Inokuti, *ibid.* **43**, 297 (1971).

[3]G. J. Schulz, Rev. Mod. Phys. **45**, 423 (1973).

[4]L. G. Christophorou and K. Siomos, in *Electron-Molecule Interactions and their Applications* (Academic, New York, 1984), Vol. 2, p. 221.

[5]L. Sanche, J. Chem. Phys. **71**, 4860 (1979).

[6]L. Sanche, G. Perluzzo, and M. Michaud, J. Chem. Phys. **83**, 3837 (1985).

[7]L. Sanche and M. Michaud, Phys. Rev. Lett. **47**, 1008 (1981).

[8]L. Sanche and M. Michaud, Phys. Rev. B **30**, 6078 (1984).

[9]L. Sanche, Phys. Rev. Lett. **53**, 1638 (1984).

[10]L. Sanche and M. Michaud, Phys. Rev. B **27**, 3856 (1983).

[11]M. Michaud and L. Sanche, Phys. Rev. B **30**, 6067 (1984).

[12]M. Michaud and L. Sanche, J. Vac. Sci. Technol. **17**, 274 (1980).

[13]G. Bader, G. Perluzzo, L. G. Caron, and L. Sanche, Phys. Rev. B **26**, 6019 (1982).

[14]A. Stamatovic and G. J. Schulz, Rev. Sci. Instrum. **41**, 423

(1970).
[15]C. Gaubert, R. Baudoing, Y. Gauthier, M. Michaud, and L. Sanche, Appl. Surf. Sci. **25**, 195 (1986).
[16]G. Perluzzo, L. Sanche, C. Gaubert, and R. Baudoing, Phys. Rev. B **30**, 4292 (1984).
[17]G. J. Schulz, Rev. Mod. Phys. **45**, 378 (1973); **45**, 423 (1973).
[18]G. Perluzzo, G. Bader, L. G. Caron, and L. Sanche, Phys. Rev. B **26**, 3976 (1982).
[19]D. C. Cartwright, A. Chutjian, S. Trajmar, and W. Williams, Phys. Rev. A **16**, 1013 (1977).
[20]D. Vichon, F. Gresteau, A. Huetz, and J. Mazeau, J. Mol. Spectrosc. **73**, 405 (1978).
[21]G. Joyez, R. I. Hall, R. Reinhardt, and J. Mazeau, J. Electron. Spectrosc. Relat. Phenom. **2**, 183 (1973).
[22]H.-J. Lau, J.-H. Fock, and E. E. Koch, Chem. Phys. Lett. **89**, 281 (1982).
[23]E. Boursey, V. Chandrasekharan, P. Gurtler, E. E. Koch, P. Kunsch, and V. Saile, Phys. Rev. Lett. **41**, 1516 (1978).
[24]M. Brith and O. Schnepp, Mol. Phys. **9**, 473 (1965).
[25]A. S. Davydov, *Theory of Molecular Excitons* (Plenum, New York, 1971).
[26]R. A. H. Buxton and W. W. Duley, Phys. Rev. Lett. **25**, 801 (1970).
[27]E. Boursey and J.-Y. Roncin, Phys. Rev. Lett. **26**, 308 (1971).
[28]J. E. Demuth, D. Schmeisser, and Ph. Avouris, Phys. Rev. Lett. **47**, 1166 (1981).
[29]L. Sanche and M. Michaud, Chem. Phys. Lett. **84**, 497 (1981).
[30]H. Ehrhardt and K. Willmann, Z. Phys. **204**, 462 (1967).
[31]M. Tronc, R. Azria, and Y. Le Coat, J. Phys. B **13**, 2327 (1980).
[32]R. M. Marsolais, L. G. Caron, G. Bader, and L. Sanche (unpublished).
[33]R. I. Hall, J. Mazeau, J. Reinhardt, and C. Schermann, J. Phys. B **3**, 991 (1970).
[34]B. Plenkiewicz, P. Plenkiewicz, G. Perluzzo, and J.-P. Jay-Gerin, Phys. Rev. B **32**, 1253 (1985).
[35]R. M. Marsolais and L. Sanche (unpublished).
[36]G. Bader, G. Perluzzo, L. G. Caron, and L. Sanche, Phys. Rev. B **30**, 78 (1984).
[37]D. S. Newman, M. Zubek, and G. C. King, J. Phys. B **16**, 2247 (1983).
[38]N. Swanson, R. J. Celotta, C. E. Kuyatt, and J. W. Cooper, J. Chem. Phys. **62**, 4880 (1975).
[39]See, for example, J. Mazeau, F. Gresteau, G. Joyez, J. Reinhardt, and R. I. Hall, J. Phys. B **5**, 1890 (1972); K. Rohr and F. Linder, J. Phys. B **9**, 2521 (1976).
[40]J. P. Gauyacq and A. Herzenberg, Phys. Rev. A **25**, 2959 (1982).
[41]M. Ohno and W. Domcke, Phys. Rev. A **28**, 3315 (1985).
[42]M. Michaud, L. Sanche, C. Gaubert, and R. Baudoing (unpublished).
[43]J. Mazeau, F. Gresteau, R. I. Hall, G. Joyez, and J. Reinhardt, J. Phys. B **6**, 862 (1973).
[44]G. Herzberg, *Molecular Spectra and Molecular Structure I* (Van Nostrand, Reinhold, New York, 1950).
[45]P. K. Carroll and C. P. Collins, Can. J. Phys. **47**, 563 (1969).
[46]*Spectroscopic Data,* edited by S. N. Suchard and J. E. Melzer (Plenum, New York, 1975, 1976), Vols. 1 and 2.
[47]J. Geiger and B. Schröder, J. Chem. Phys. **50**, 7 (1968).
[48]A. Chutjian, D. C. Cartwright, and S. Trajmar, Phys. Rev. Lett. **30**, 195 (1973).
[49]R. Haensel, E. E. Koch, N. Kosuch, U. Nielsen, and M. Skibowski, Chem. Phys. Lett. **9**, 548 (1971).
[50]S. Daviel, B. Wallbank, J. Comer, and P. J. Hicks, J. Phys. B **15**, 1929 (1982).